CKJ REVIEW

Non-invasive approaches in the diagnosis of acute rejection in kidney transplant recipients. Part I. *In vivo* imaging methods

Oriane Hanssen[1,*], Pauline Erpicum[1,2,*], Pierre Lovinfosse[3], Paul Meunier[4], Laurent Weekers[1], Luaba Tshibanda[4], Jean-Marie Krzesinski[1,2], Roland Hustinx[3], and François Jouret[1,2]

[1]Division of Nephrology, University of Liège Academic Hospital (ULg CHU), Avenue Hippocrate, 13, B-4000 Liège, Belgium, [2]GIGA Cardiovascular Sciences, University of Liège, Liège, Belgium, [3]Division of Nuclear Medicine, University of Liège Academic Hospital (ULg CHU), Liège, Belgium, and [4]Division of Radiology, University of Liège Academic Hospital (ULg CHU), Liège, Belgium

Correspondence and offprint requests to: François Jouret; E-mail: francois.jouret@chu.ulg.ac.be

Abstract

Kidney transplantation (KTx) represents the best available treatment for patients with end-stage renal disease. Still, full benefits of KTx are undermined by acute rejection (AR). The diagnosis of AR ultimately relies on transplant needle biopsy. However, such an invasive procedure is associated with a significant risk of complications and is limited by sampling error and interobserver variability. In the present review, we summarize the current literature about non-invasive approaches for the diagnosis of AR in kidney transplant recipients (KTRs), including *in vivo* imaging, gene expression profiling and omics analyses of blood and urine samples. Most imaging techniques, like contrast-enhanced ultrasound and magnetic resonance, exploit the fact that blood flow is significantly lowered in case of AR-induced inflammation. In addition, AR-associated recruitment of activated leukocytes may be detectable by ^{18}F-fluoro-deoxy-glucose positron emission tomography. In parallel, urine biomarkers, including CXCL9/CXCL10 or a three-gene signature of CD3ε, IP-10 and 18S RNA levels, have been identified. None of these approaches has been adopted yet in the clinical follow-up of KTRs, but standardization of procedures may help assess reproducibility and compare diagnostic yields in large prospective multicentric trials.

Key words: 18FDG-PET/CT, acute rejection, kidney biopsy, kidney transplantation, magnetic resonance imaging, ultrasonography

Introduction

Kidney transplantation (KTx) represents the best available treatment for patients with end-stage renal disease. Each year, 3.500 kidney transplants are performed in the EuroTransplant zone (www.eurotransplant.org). Still, full benefits of KTx are regrettably undermined by acute rejection (AR), which may be cellular

or antibody-mediated [1]. AR may affect all kidney transplant recipients (KTRs) throughout their lifetime, independent of age or gender [2]. Furthermore, subclinical AR affects 10–30% of KTRs within the first year following KTx and is an early predictor of subsequent graft failure [3, 4]. Subclinical AR has been defined as 'the documentation by light histology of unexpected evidence of AR in a stable patient' and concerns 5–10% of patients without high immunological risk. Hence, most transplant centres routinely perform 'surveillance' transplant biopsies between 3 and 12 months post-KTx. Since current immunosuppressive drugs efficiently treat AR, diagnosing AR early is crucial. Of note, it is still not debated whether subclinical AR should be treated or not. Although some centres treat subclinical AR, others do not compulsively treat it because of the lack of strong evidence about the risk–benefit balance of increased immunosuppression. In a 10-year observational prospective cohort study of 1001 consecutive non-selected KTRs who underwent ABO-compatible, complement-dependent, cytotoxicity-negative crossmatch KTx and who underwent screening biopsies at 1 year, treatment of subclinical T-cell-mediated AR resulted in similar long-term graft survival as in patients without rejection [4]. In contrast, subclinical antibody-mediated AR detected at the 1-year screening biopsy carried a negative prognostic value independent of initial donor-specific antibody status, previous immunologic events, estimated glomerular filtration rate (eGFR) and proteinuria.

In clinical practice, the detection of AR critically depends on periodic assessments of serum creatinine (SCr), an insensitive measure of renal injury, together with clinical signs like oedema or hypertension [5]. Ultimately, diagnosis of AR relies on transplant needle biopsy. Examining kidney samples by light microscopy provides well-characterized and gold-standard criteria for renal AR summarized in the conventional Banff classification [2, 6]. However, such an invasive procedure may cause graft bleeding or arteriovenous fistula. In addition, distinct reports based on former pathology classification [7] or frozen pre-implantation biopsies [8] highlighted sampling error and interobserver variability. Moreover, repeated biopsies to evaluate the renal graft's status pose challenges, including practicability and cost. Therefore, alternative, less invasive but highly sensitive modalities are currently under investigation to reinforce our armamentarium in the diagnosis of AR [1, 9–15]. Likewise, it would be useful to non-invasively predict non-rejection in KTRs with acute renal dysfunction and suspected AR in order to avoid needless transplant biopsy. The term 'acute dysfunction with no rejection' (ADNR) has been recently proposed by Kurian *et al.* [16] to reflect such a frequent condition in which AR is suspected on the basis of clinical and biological judgments, but not confirmed by histology. The mechanisms and long-term consequences of ADNR remain unknown.

In the present review, we summarize the current literature about non-invasive approaches for the diagnosis of AR in KTRs, with a particular emphasis on *in vivo* imaging methods. The benefits and limitations of gene expression profiling and omic analyses of blood and urine samples in the non-invasive diagnosis of renal AR are reviewed in a complementary Part II article. Most imaging techniques exploit the fact that blood flow is significantly lowered in case of AR-induced inflammation. Indeed, AR is associated with a recruitment of activated leukocytes into the transplant, with the release of vasoactive mediators, such as endothelin, leukotrienes, thromboxane A2 and LG3 (C-terminal fragment of perlecan) [17, 18]. In addition, activated leukocytes are characterized by an increased avidity for glucose and its radiolabelled analogue, 18F-fluoro-deoxy-glucose (^{18}F-FDG). Such an accumulation of ^{18}F-FDG is detectable by positron emission tomography (PET), as demonstrated in both rat and man [15, 19].

Ultrasound

Ultrasound (US) is based on the 'Doppler effect', which stipulates that US reflected from moving structures changes its frequency. The main advantages of US include rapidity and the absence of radiation or injections of nephrotoxic contrast agent. Conversely, US is highly operator dependent and the interpretation may be significantly influenced by extra-renal factors, such as age, body mass index, atherosclerosis and arterial stiffness. In severe AR, duplex colour Doppler US shows a spectral waveform in which the diastolic arterial flow is decreased (Figure 1) [20]. Consequently, evaluation of the renal transplant resistance index (RI) may help detect acute graft dysfunction [21–23]. However, RI measurements cannot differentiate AR from acute tubular necrosis (ATN), calcineurin inhibitor toxicity, renal vein thrombosis, ureteral obstruction or pyelonephritis [22]. In case of delayed graft function (DGF) [24], sequential Doppler US does not help specifically detect AR. In 2014, Shebel *et al.* [25] suggested that power Doppler may distinguish ATN with preserved cortical perfusion from AR with reduced perfusion. Power Doppler is based
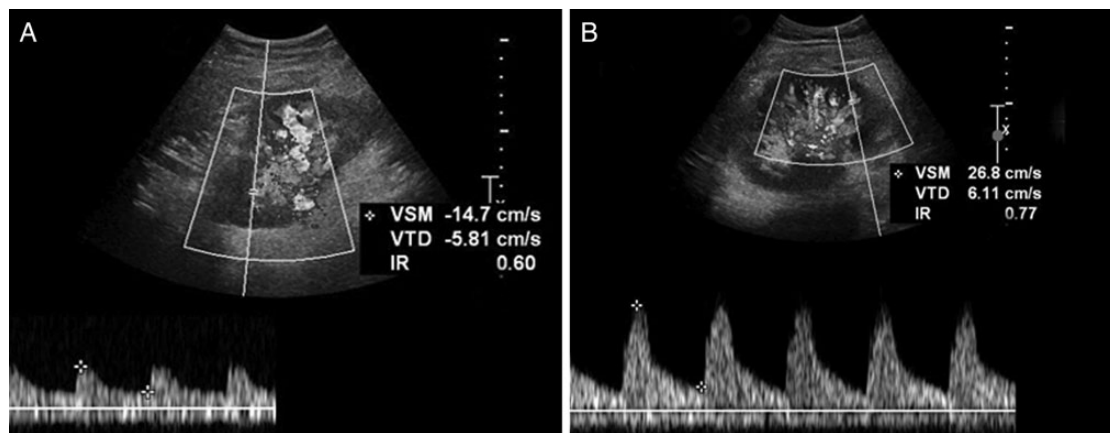

Fig. 1. Representative Doppler ultrasound imaging in case of biopsy-proven renal allograft acute rejection. Doppler ultrasound images of a renal allograft (from the same kidney transplant recipient) (**A**) without versus (**B**) with biopsy-proven acute rejection (AR). The index of resistance (IR; normal value <0.70) of renal parenchyma is significantly increased in the case of AR (B). VSM, maximal systolic velocity; VTD, telediastolic velocity.

on the amplitude of the Doppler signal to detect moving matter. This procedure is independent of flow direction—thereby excluding signal aliases—and is independent of angle—thereby allowing detection of smaller velocities than colour Doppler [23, 26, 27]. The role of power Doppler in the diagnosis of AR remains controversial [28, 29] and additional investigations are required to assess its sensitivity/specificity and predictive values (Table 1).

Molecular imaging techniques specifically targeting T-lymphocytes represent another promising tool for the detection of AR. Grabner et al. [30] recently performed a study using antibody-mediated contrast-enhanced US (CEUS) using microbubbles targeting CD3-, CD4- or CD8-positive T-cells in various murine models of kidney diseases. The results of CEUS correlated with histopathological scoring of rejection, CD3 immuno-signal and mRNA expression levels of chemoattractant cytokines. Signal intensities reflected the degree of inflammation in the allograft as early as 2 days after KTx. Conversely, ATN and CSA toxicity were not associated with increased CEUS signals. Thus, CD3-mediated CEUS may help specifically detect renal AR. Further preclinical and clinical studies are warranted to assess the diagnostic yield of CEUS in real-life settings since infection-induced infiltration of T-lymphocytes may represent an important confounding factor [30].

Computed tomography

Computed tomography (CT) uses X-rays to create pictures of cross sections of the body. Perfusion techniques are based on the injection of iodinated contrast agents (Table 1). In 2013, Helck et al. [31] retrospectively suggested that studying perfusion of kidney allografts by CT may help non-invasively differentiate AR from ATN. Twenty-two patients with either AR ($n = 6$) or ATN ($n = 16$) were included. There was no significant difference regarding SCr levels between groups. All patients underwent a multiphase CT angiography, which showed that renal blood flow values were significantly lower in allografts with biopsy-proven AR (48.3 ± 21 mL/100 mL/min) in comparison to those with ATN (77.5 ± 21 mL/100 mL/min) [32]. The mean effective radiation dose of the CT perfusion protocol was 13.6 ± 5.2 mSv. Further investigations are necessary to assess the clinical relevance of this quantitative perfusion technique in discriminating the various causes of acute graft dysfunction, taking into account the radiation exposure and the risk of contrast-induced nephropathy (which promotes the persistence of ATN).

Magnetic resonance imaging

Magnetic resonance imaging (MRI) derives from the radiofrequency signal generated by hydrogen atoms placed in an external magnetic field. The main advantages of contrast-enhanced MRI after infusion of gadolinium-based agents include high-contrast resolution and the absence of ionizing radiation. KTRs with biopsy-proven AR show a lower cortical enhancement with delayed renal excretion (Table 1). Many reports have qualitatively evaluated the shape of the renal enhancement curve to diagnose acute dysfunction. As early as 1997, Szolar et al. [33] performed a study including 23 patients with clinically suspected ATN or AR and 8 consecutive control patients, who underwent MR perfusion imaging of renal allograft. The increase in cortical signal intensity was significantly smaller in patients with AR ($61 \pm 4\%$ increase above baseline) compared with that measured in normal allografts ($136 \pm 9\%$ increase above baseline) and patients with ATN ($129 \pm 3\%$ increase above baseline) [33–38]. It should be noted, the administration of gadolinium-based contrast

agents has been associated with nephrogenic systemic fibrosis, a devastating fibrosing disorder of the skin and other systemic organs. Their use is therefore prohibited in patients with acute kidney injury (AKI) or stage 4/5 chronic kidney disease, as well as in KTRs [39, 40].

Innovative applications of MRI avoiding gadolinium-based agents have been recently developed (Table 1). Diffusion-weighted imaging (DWI) provides quantification of the Brownian motion of water protons by calculating the apparent diffusion coefficient (ADC) [41–44]. Several studies have shown that ADC in patients with stable renal function is significantly higher than in patients with kidney dysfunction [41, 42, 44]. The diagnostic accuracy of ADC evaluation in detecting acute renal allograft dysfunction is high, although the specificity in AR diagnosis is low [41–43]. Indeed, ADC can be lowered in various conditions, like ATN, drug toxicity and ischaemia [41, 42, 44]. Arterial spin labelling (ASL) is another non-invasive functional MRI approach that allows one to quantify renal perfusion without administration of contrast agents by labelling water protons of the arterial blood with radiofrequency pulses [45]. A recent study conducted by Hueper et al. [45] demonstrated that renal perfusion was significantly reduced in patients with DGF. Forty-six patients underwent contrast-free ASL MRI 4 to 11 days after KTx. Renal biopsies were performed within 5 days of MRI. Twenty-six of 46 patients developed DGF. Of these, nine patients had biopsy-proven AR. Renal perfusion was significantly lower in the DGF group compared with the control group (231 ± 15 versus 331 ± 15 mL/min/100 g). Renal perfusion significantly correlated with eGFR, RI and cold ischaemia time. Note that ASL is not available in routine clinical practice. Finally, blood oxygenation level-dependent (BOLD) imaging uses deoxygenated haemoglobin as an endogenous contrast agent. When the blood concentration of deoxyhemoglobin increases, the $T2^*$ relaxation time of the protons decreases, which increases dephasing in the surrounding tissues. $R2^*$ corresponds to $1/T2^*$, and is an index of the signal loss rate [40, 46–50]. Decreased $R2^*$ values in the renal medulla correspond to increased oxygen concentration. Hence, BOLD imaging may help differentiate AR from ATN [43–45, 51]. Han et al. [34] showed that allografts with ATN have decreased oxygen bioavailability in early stages. Eighty-two patients with normal graft function and 28 patients with biopsy-proven AR ($n = 21$) or ATN ($n = 7$) were enrolled. Patients with AR and ATN underwent BOLD MRI within 6 days before or after kidney transplant biopsy. The mean cortical $R2^*$ level was significantly higher in the ATN group (15.25 ± 1.03/s) compared with the normal group (13.35 ± 2.31/s) and the AR group (12.02 ± 1.72/s). However, such an observation was not confirmed by Djamali et al. [52], most probably because of the complex definition of ATN stages [51]. Furthermore, oxygenation is dynamic and may be influenced by a number of local and systemic stimuli, including drugs [46–49, 51].

Besides these innovative MRI applications based on endogenous contrast materials, ultrasmall superparamagnetic iron oxide (USPIO)-enhanced dynamic MRI tracks macrophage accumulation in various tissues and organs, including kidney transplant (Table 1). In vivo experimental USPIO studies have been performed in rats. USPIO particles are trapped by macrophages through absorptive endocytosis, which creates MR signal reduction in $T2^*$-weighted images [53–57]. Although sensitive, USPIO-enhanced dynamic MRI is characterized by poor specificity since image hypointensity may result from sources other than labelled cells [53–55]. Moreover, it may be difficult to differentiate AR from infection or ischaemic injury, which are also known to be associated with macrophage recruitment [53–58].

Table 1. Characteristics of imaging approaches used in the diagnosis of kidney allograft acute rejection

		Images in AR	Availability in humans	Sensitivity and specificity	Advantages	Disadvantages
Ultrasound	Colour Doppler	– Reversed diastolic arterial flow – ↑RI	Yes	Se 40% Sp 62% [29]	– Rapid – Non-invasive – No radiation – No contrast	– Operator dependence – Influence of extra-renal factors
	Power Doppler	↓ cortical perfusion	Yes	Se 40% [28]/82% [25] Sp 100% [25, 28]	– Independent of velocity, direction of flow and angle – Functional prognosis	
	CEUS	↑ signal intensity	No	High Sp versus ATN-CSA High Sp versus CSA toxicity Poor Sp versus infections [30]	Feasible as early as 2 days post transplantation	
CT	Perfusion CT	↓ renal blood flow	Yes	Unknown [31]		– Radiation exposure – Contrast-induced nephropathy
MRI	Contrast-enhanced MRI	– ↓ cortical enhancement – Delayed renal excretion	Yes	Unknown	– High-contrast resolution – No radiation	Nephrogenic systemic fibrosis
	Diffusion-weighted MRI	↓ ADC	Under-development	Se 90%/Sp: conflicting – 95.9% [41] – low [42]	– Endogenous material as contrast agents – Functional contrast-free MRI	
	Arterial spin labelling	↓ renal perfusion	Under development	Unknown		
	BOLD imaging	↓ R2* values in medulla	Under-development	Se 80% [46], 96.4% [47] Sp 72% [46], 74.4% [47]		
	USPIO-enhanced dynamic MRI	Hypointensity on T*2-weighted images	Yes	Unknown		

Modality	Technique		Tracer	Parameters	Availability	Performance	Advantages	Limitations
Nuclear imaging	Scintigraphy	Dynamic	^{99m}Tc DTPA MAG3	Flat uptake curves Decreased perfusion	Yes	Sp 87.9% [59]	3D – Significant tissue penetration of conventional tracers – Ability to detect very low accumulation of tracers – Functional images – Absence of nephrotoxicity	– High radiation exposure – Poor image quality
		Static ± SPECT	Ga-Ci	↑ signal intensity	Yes	Poor specificity [60]		– Useless in necrosis or in case of high doses of heparin
			^{99m}T-SC	No influence of renal function		Se 93.3% Sp 44.4% [9]		– Accumulation in lungs – Variation of labeling stability – Limitation of interpretation from background activity
			Radiolabelled WBCs		Yes (in some facilities)	PPV 100% NPV 95.1% [61]		– Allergic reactions – Restricted exploration to intra- and perivascular antigens
			Radiolabelled monoclonal Ab		Yes	Unknown [13]		
	PET-CT		^{18}F-FDG PET-CT	↑ value of the mean SUV	Yes	Se 100% Sp 50% [15]		– Non-specific tracer – Late acquisitions – Cost –
			^{18}F-FDG-labelled WBCs	production	Unknown [62]		– ↓ radiation dose – Early acquisition	– Laborious production

AR, acute rejection; CT, computed tomography; MRI, magnetic resonance imaging; RI, resistance index; Se, sensitivity; Sp, specificity; SUV, standard uptake value; Ga-Ci: ^{67}Ga-citrate; ^{99m}TSC: ^{99m}Tc-sulfur colloid; WBCs, white blood cells; Ab, antibodies; PPV, positive predictive value; NPV, negative predictive value.

Renal scintigraphy

Planar scintigraphy detects, with a γ camera, the distribution of radioactivity after administration of a γ photon-emitting radio-pharmaceutical agent (Table 1). Single photon emission computed tomography (SPECT) intrinsically offers high intrinsic activity due to (i) the significant tissue penetration of conventional tracers, (ii) the ability to detect very low accumulations of tracers and (iii) the large range of available radiotracers [13, 63]. In addition, nuclear imaging is largely operator independent and generates three-dimensional (3D) functional images of metabolic processes covering the whole organ/body (upon the technique used). Radiotracers for renal scintigraphy are devoid of nephrotoxicity [13, 55]. In the particular case of AR, SPECT-based approaches may detect the recruitment of activated leukocytes into the transplant [13].

Dynamic renal scintigraphy with ^{99m}Tc-DTPA or MAG3 shows poor specificity for AR diagnosis [21, 64–66]. Aktas et al. [36] suggested that serial radionuclide imaging may help distinguish parenchymal causes of graft failure. This retrospective study included 32 patients with acute renal allograft dysfunction. In patients with AR, at least two sets of serial images were obtained after intravenous injection of 340 MBq of ^{99m}Tc-DTPA. Sensitivity and specificity were high in the diagnosis of AR. Sensitivity was even higher when considering the perfusion curve after the peak (P/PL) rather than measuring the curve from start to peak (Hilson's PI) [59]. Indeed, the major pathophysiologic difference between AR and ATN concerns renal blood flow, which is significantly impaired in AR but relatively well-preserved in ATN [59].

Besides dynamic scintigraphy, static imaging using radiotracers accumulating in renal parenchyma, like ^{67}Ga-citrate, ^{125}I-fibrinogen and ^{99m}Tc-sulfur colloid, have been studied in AR. Although comparative meta-analysis suggested a similar specificity of these tracers in AR [60], ^{99m}Tc-sulfur colloid might be the only one operational in clinical settings within the permissible radiation dose. ^{67}Ga-citrate accumulates in the polymorphonuclear granulocytes recruited to inflammatory lesions, with no differential specificity between bacterial or sterile inflammation and AR [60]. Iodinated fibrinogen has been shown to deposit along the vascular system and into renal interstitium in case of AR [60, 63, 64]. In 1976, Niederle et al. [67] performed a prospective study on 22 patients using ^{125}I-fibrinogen. The uptake of radiolabelled fibrinogen was increased in all biopsy-proven AR. Histologically, the kidneys with increased accumulation of fibrinogen showed extensive deposits of fibrin in blood vessels, glomeruli, intracapillary thrombi and interstitium [63]. However, ^{125}I is not suited for scintigraphic imaging, and this tracer has never been used in routine clinical practice [60]. Finally, ^{99m}Tc-sulfur colloid is trapped in fibrin thrombosis associated with AR [9, 60]. The accumulation of ^{99m}Tc-sulfur colloid in kidney grafts is independent of renal function. Imaging after infusion of ^{99m}Tc-sulfur colloid appeared to discriminate AR on the basis of a strictly visual scale [9]. Unfortunately, several studies using computer-assisted quantification of allograft uptake compared with the surrounding pelvis showed conflicting results, with false-negative and false-positive rates that were too high to make ^{99m}Tc-sulfur colloid useful in predicting renal AR in routine clinical practice [65]. Furthermore, ^{99m}Tc-sulfur colloid does not accumulate in cases of AR-associated necrosis or in patients receiving high doses of heparin [60].

Several experimental and clinical pilot trials have been performed using radiolabelled white blood cells (WBCs) to detect renal AR, with conflicting results [13, 63, 70]. Preclinical tests using ex vivo radiolabelled leukocytes highlighted significant

translational limitations (Table 1). First, labelled WBCs briefly accumulate in the lungs. Second, labelling stability varies. Third, the compound stability of the tracer and radionuclide half-life have to be taken into account before reliably measuring the accumulation of labelled leukocytes [13, 55]. Finally, background activity as well as the degree of attenuation of target organ activity may limit the interpretation [66]. In 2004, Lopes de Souza *et al.* [38] used ^{99m}Tc-labelled WBCs to evaluate AR in KTRs. This prospective study enrolled 100 KTRs. Scintigraphy detected 13 of 16 biopsy-proven ARs and 4 of 5 ATNs, which corresponds to a sensitivity of 81% for AR and 80% for ATN. The specificity was 100%. The positive predictive value was 100% and the negative predictive value was 95.1 and 98.9% for AR and ATN, respectively. Similarly, radiolabelled monoclonal antibodies directed against infiltrating cells have also been used. Anti-CD3 (cytotoxic T-cells), anti-CD4 (helper T-cells), anti-CD20 (B-cells), anti-CD25 (T- and B-cells), anti-DR (antigen-presenting cells) or anti-granulocyte have been tested to assess inflammation. Application of radiolabelled anti-CD3 or anti-CD25 might be promising in the particular settings of AR [59]. Still, this technique may cause allergic reactions and is restricted to intra- and perivascular antigens since antibodies do not cross the endothelial barrier [13, 63].

Positron emission tomography

PET detects pairs of γ rays indirectly emitted by positron emitting radionuclides, like ^{18}F-FDG. PET/CT offers a direct 3D co-registration with low-dose CT without administration of contrast medium. ^{18}F-FDG PET/CT is routinely used for detection, characterization, staging and follow-up of inflammatory processes of various origins [71, 72]. Activated leukocytes are indeed characterized by high metabolic activity and increased uptake of glucose and its analogue, ^{18}F-FDG (Table 1). Renal AR is associated with a recruitment of activated leukocytes into the transplant, which is the basis of the Banff classification [6]. The advantages of ^{18}F-FDG-PET/CT are rapid imaging and a high target:background ratio [72]. It can be used safely in patients with renal function ranging from normal to mildly reduced GFR to ESRD. In rats, the renal clearance of ^{18}F-FDG does not correlate with renal function [19]. In particular, acute kidney injury secondary to cyclosporin exposure or ischaemia/reperfusion (I/R) is not associated with significant elevation in renal ^{18}FDG accumulation. In man, Minamimoto *et al.* [73] investigated the influence of renal function on ^{18}F-FDG distribution and uptake in 20 normal volunteers and 20 patients with suspected renal failure. Regions of interest were placed over 15 different regions throughout the body, including the left kidney. No significant difference was observed in the renal mean standard uptake value (SUV) between healthy volunteers and patients with suspected renal failure. Limitations of ^{18}F-FDG-PET/CT imaging include its cost and availability, as well as the exposure to radiation originating from both PET and CT procedures. Still, a cumulative exposure dose of ~5 mSv remains low compared with other classical radiological exams, like thorax CT (7 mSv) or abdomen CT (8 mSv) or coronary angiography (16 mSv) [15, 74]. The uptake of ^{18}F-FDG is not specific for inflammation and may be increased in other conditions, like tumours or infections [71, 75]. Furthermore, physiological urinary excretion of ^{18}F-FDG may hamper the measurement of ^{18}FDG uptake in the renal parenchyma [76]. Late acquisitions may help overcome this problem and eventually improve the background:noise ratio. One rodent model of allogeneic KTx suggested that ^{18}F-FDG PET/CT non-invasively detects renal cellular-mediated AR

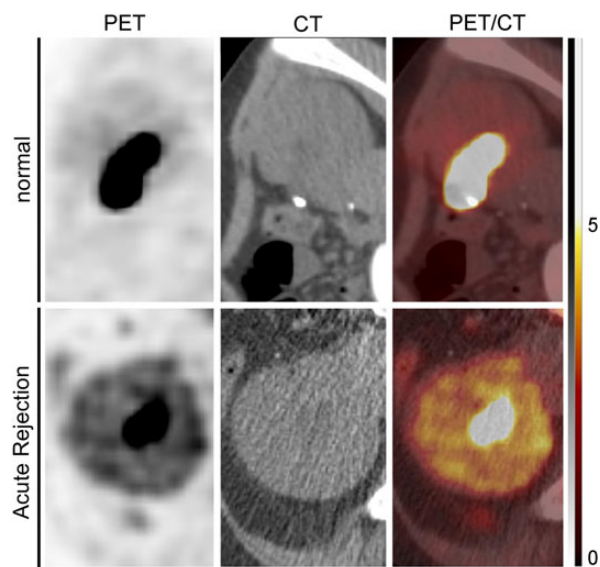**Fig. 2.** Representative ^{18}F-FDG PET/CT imaging in case of biopsy-proven renal allograft acute rejection. Positron-emission tomography (PET; left column), computed tomography (CT; middle column) and combined PET/CT images taken ~180 min after intravenous administration of ^{18}fluoro-deoxy-glucose (^{18}FDG) are shown for one kidney transplant recipient (KTR) with normal renal histology (upper panels) and one KTR with biopsy-proven acute rejection (AR). The tracer, ^{18}FDG, significantly accumulates in the renal parenchyma in case of AR. Note the detection of excreted ^{18}FDG in the urinary pelvis in both normal and pathological situations. The arbitrary scale of the standard uptake value (from 0 to 5) is illustrated on the right side.

[19, 51]. Recently, we have prospectively shown the usefulness of ^{18}F-FDG PET/CT in KTRs presenting with suspected AR prompting a transplant biopsy (Figure 2) [15]. On the basis of 32 ^{18}FDG-PET/CTs in 31 adult KTRs, we found a positive correlation between ^{18}F-FDG transplant uptake (i.e. mean SUV) and the acute composite Banff score of leukocyte infiltration ($r^2 = 0.49$). The area under the receiver operating characteristic (ROC) curve (AUC) was 0.93, with 100% sensitivity and 50% specificity, using a mean SUV threshold of 1.6. The poor specificity of ^{18}F-FDG PET/CT in detecting AR is primarily due to the nature of the radiotracer. Although supporting a role for ^{18}F-FDG PET/CT in AR screening, these preliminary data raise many unresolved issues, including (i) the dynamics of transplant ^{18}F-FDG uptake, (ii) the comparative yield of ^{18}F-FDG PET/CT in cellular- versus antibody-mediated AR, (iii) the predictive value of transplant ^{18}F-FDG uptake on long-term renal function and (iv) the yield of ^{18}FDG-PET/CT in subclinical AR.

Grabner *et al.* [39] investigated the diagnostic yield of ^{18}F-FDG-labelled T lymphocytes in a rat model of allogenic KTx (Table 1). The accumulation of labelled T-cells was significantly elevated in allografts with AR [1.07 ± 0.28% of injected dose (ID)] compared with to native control kidneys (0.49 ± 0.18% ID). No difference was found among native controls, CSA toxicity and kidneys with I/R injury. To validate PET data, they showed significant correlations between imaging-based *in vivo* measurements of T-cell accumulation with autoradiography, histology and PCR quantifications. The use of radiolabelled cells has several advantages, such as higher sensitivity with a minimum radiation dose and less urinary excretion of free ^{18}F-FDG, which enables early acquisition and quantification. However, the production of radiolabelled leukocytes in man would be laborious and time-consuming.

Conclusions and perspectives

Renal AR remains one of the leading causes of reversible acute dysfunction in KTRs and is an early predictor of subsequent graft failure [3, 4]. The diagnosis and classification of AR ultimately rely on transplant needle biopsy. Indeed, the current imaging procedures do not differentiate AR subtypes and therefore do not help in adjusting immunosuppressive therapies. However, imaging may be useful in the early detection of AR, thereby quickening and improving KTR management, as well as in the follow-up of biopsy-proven AR subtypes. Importantly, the non-invasive discrimination of AR from ADNR, with the highest negative predictive value, would help avoid needless and risky transplant biopsies. On the basis of the current literature, MRI and ^{18}F-FDG PET/CT appear the most promising approaches. Nevertheless, none of these has been adopted yet in routine clinical practice. This may be partly explained by methodological and financial limitations. Standardization and validation of analysis procedures are urgently required to assess reproducibility in prospective multicentric trials. Furthermore, additional studies should focus on the diagnostic yields of combinations of imaging and omics methods.

Conflict of interest statement

The authors have no conflicts of interest to report. This manuscript has not been previously published elsewhere, in whole or in part.

References

1. Suthanthiran M, Schwartz JE, Ding R et al. Urinary-cell mRNA profile and acute cellular rejection in kidney allografts. N Engl J Med 2013; 369: 20–31
2. Williams WW, Taheri D, Tolkoff-Rubin N et al. Clinical role of the renal transplant biopsy. Nat Rev Nephrol 2012; 8: 110–121
3. Rush D, Nickerson P, Gough J et al. Beneficial effects of treatment of early subclinical rejection: a randomized study. J Am Soc Nephrol 1998; 9: 2129–2134
4. Loupy A, Vernerey D, Tinel C et al. Subclinical rejection phenotypes at 1 year post-transplant and outcome of kidney allografts. J Am Soc Nephrol 2015; 26: 1721–1731
5. Thomas ME, Blaine C, Dawnay A et al. The definition of acute kidney injury and its use in practice. Kidney Int 2015; 87: 62–73
6. Haas M, Sis B, Racusen LC et al. Banff 2013 meeting report: inclusion of C4d-negative antibody-mediated rejection and antibody-associated arterial lesions. Am J Transplant 2014; 14: 272–283
7. Furness PN, Taub N. International variation in the interpretation of renal transplant biopsies: report of the CERTPAP Project. Kidney Int 2001; 60: 1998–2012
8. Azancot MA, Moreso F, Salcedo M et al. The reproducibility and predictive value on outcome of renal biopsies from expanded criteria donors. Kidney Int 2014; 85: 1161–1168
9. Einollahi B, Bakhtiari P, Simforoosh N et al. Renal allograft accumulation of technetium-99m sulfur colloid as a predictor of graft rejection. Transplant Proc 2005; 37: 2973–2975
10. Khalifa F, Beache GM, El-Ghar MA et al. Dynamic contrast-enhanced MRI-based early detection of acute renal transplant rejection. IEEE Trans Med Imaging 2013; 32: 1910–1927
11. Blydt-Hansen TD, Sharma A, Gibson IW et al. Urinary metabolomics for noninvasive detection of borderline and acute T cell-mediated rejection in children after kidney transplantation. Am J Transplant 2014; 14: 2339–2349
12. Ong S, Mannon RB. Genomic and proteomic fingerprints of acute rejection in peripheral blood and urine. Transplant Rev 2015; 29: 60–67
13. Pawelski H, Schnöckel U, Kentrup D et al. SPECT- and PET-based approaches for noninvasive diagnosis of acute renal allograft rejection. Biomed Res Int 2014; 2014: 874785
14. Hirt-Minkowski P, De Serres SA, Ho J. Developing renal allograft surveillance strategies—urinary biomarkers of cellular rejection. Can J Kidney Health Dis 2015; 2: 28
15. Lovinfosse P, Weekers L, Bonvoisin C et al. Fluorodeoxyglucose F(18) positron emission tomography coupled with computed tomography in suspected acute renal allograft rejection. Am J Transplant 2015; 16: 310–316
16. Kurian SM, Williams AN, Gelbart T et al. Molecular classifiers for acute kidney transplant rejection in peripheral blood by whole genome gene expression profiling. Am J Transplant 2014; 14: 1164–1172
17. Spurney RF, Ibrahim S, Butterly D et al. Leukotrienes in renal transplant rejection in rats. Distinct roles for leukotriene B4 and peptidoleukotrienes in the pathogenesis of allograft injury. J Immunol 1994; 152: 867–876
18. Soulez M, Pilon E-A, Dieudé M et al. The perlecan fragment LG3 is a novel regulator of obliterative remodeling associated with allograft vascular rejection. Circ Res 2012; 110: 94–104
19. Reuter S, Schnöckel U, Schröter R et al. Non-invasive imaging of acute renal allograft rejection in rats using small animal F-FDG-PET. PLoS One 2009; 4: e5296
20. Brown ED, Chen MY, Wolfman NT et al. Complications of renal transplantation: evaluation with US and radionuclide imaging. Radiographics 2000; 20: 607–622
21. Burgos FJ, Pascual J, Marcen R et al. The role of imaging techniques in renal transplantation. World J Urol 2004; 22: 399–404
22. Cano H, Castañeda DA, Patiño N et al. Resistance index measured by Doppler ultrasound as a predictor of graft function after kidney transplantation. Transplant Proc 2014; 46: 2972–2974
23. Kocabaș B, Aktas A, Aras M et al. Renal scintigraphy findings in allograft recipients with increased resistance index on Doppler sonography. Transplant Proc 2008; 40: 100–103
24. Mallon DH, Summers DM, Bradley JA et al. Defining delayed graft function after renal transplantation: simplest is best. Transplantation 2013; 96: 885–889
25. Shebel HM, Akl A, Dawood A et al. Power Doppler sonography in early renal transplantation: does it differentiate acute graft

rejection from acute tubular necrosis? *Saudi J Kidney Dis Transpl* 2014; 25: 733–740

26. Chow L, Sommer FG, Huang J *et al*. Power Doppler imaging and resistance index measurement in the evaluation of acute renal transplant rejection. *J Clin Ultrasound* 2001; 29: 483–490

27. Wang H-K, Chou Y-H, Yang A-H *et al*. Evaluation of cortical perfusion in renal transplants: application of quantified power Doppler ultrasonography. *Transplant Proc* 2008; 40: 2330–2332

28. Sidhu MK, Gambhir S, Jeffrey RB *et al*. Power Doppler imaging of acute renal transplant rejection. *J Clin Ultrasound* 1999; 27: 171–175

29. Trillaud H, Merville P, Tran Le Linh P *et al*. Color Doppler sonography in early renal transplantation follow-up: resistive index measurements versus power Doppler sonography. *AJR Am J Roentgenol* 1998; 171: 1611–1615

30. Grabner A, Kentrup D, Pawelski H *et al*. Renal contrast-enhanced sonography findings in a model of acute cellular allograft rejection. *Am J Transplant* 2016; 16: 1612–1619

31. Helck A, Wessely M, Notohamiprodjo M *et al*. CT perfusion technique for assessment of early kidney allograft dysfunction: preliminary results. *Eur Radiol* 2013; 23: 2475–2481

32. Sebastià C, Quiroga S, Boyé R *et al*. Helical CT in renal transplantation: normal findings and early and late complications. *Radiographics* 2001; 21: 1103–1117

33. Szolar DH, Preidler K, Ebner F *et al*. Functional magnetic resonance imaging of human renal allografts during the post-transplant period: preliminary observations. *Magn Reson Imaging* 1997; 15: 727–735

34. Hricak H, Terrier F, Marotti M *et al*. Posttransplant renal rejection: comparison of quantitative scintigraphy, US, and MR imaging. *Radiology* 1987; 162: 685–688

35. Khalifa F, Abou El-Ghar M, Abdollahi B *et al*. A comprehensive non-invasive framework for automated evaluation of acute renal transplant rejection using DCE-MRI. *NMR Biomed* 2013; 26: 1460–1470

36. Khalifa F, El-Baz A, Gimel'farb G *et al*. Non-invasive image-based approach for early detection of acute renal rejection. *Med Image Comput Comput Assist Interv* 2010; 13: 10–18

37. Onniboni M, De Filippo M, Averna R *et al*. Magnetic resonance imaging in the complications of kidney transplantation. *Radiol Med* 2013; 118: 837–850

38. Yamamoto A, Zhang JL, Rusinek H *et al*. Quantitative evaluation of acute renal transplant dysfunction with low-dose three-dimensional MR renography. *Radiology* 2011; 260: 781–789

39. Perazella MA, Reilly RF. Nephrogenic systemic fibrosis: recommendations for gadolinium-based contrast use in patients with kidney disease. *Semin Dial* 2008; 21: 171–173

40. Abu-Alfa AK. Nephrogenic systemic fibrosis and gadolinium-based contrast agents. *Adv Chronic Kidney Dis* 2011; 18: 188–198

41. Abou-El-Ghar ME, El-Diasty Ta, El-Assmy aM *et al*. Role of diffusion-weighted MRI in diagnosis of acute renal allograft dysfunction: a prospective preliminary study. *Br J Radiol* 2012; 85: e206–e211

42. Kaul A, Sharma RK, Gupta RK *et al*. Assessment of allograft function using diffusion-weighted magnetic resonance imaging in kidney transplant patients. *Saudi J Kidney Dis Transpl* 2014; 25: 1143–1147

43. Eisenberger U, Thoeny HC, Binser T *et al*. Evaluation of renal allograft function early after transplantation with diffusion-weighted MR imaging. *Eur Radiol* 2010; 20: 1374–1383

44. Park SY, Kim CK, Park BK *et al*. Assessment of early renal allograft dysfunction with blood oxygenation level-dependent MRI and diffusion-weighted imaging. *Eur J Radiol* 2014; 83: 2114–2121

45. Hueper K, Gueler F, Bräsen JH *et al*. Functional MRI detects perfusion impairment in renal allografts with delayed graft function. *Am J Physiol Renal Physiol* 2015; 308: F1444–F1451

46. Han F, Xiao W, Xu Y *et al*. The significance of BOLD MRI in differentiation between renal transplant rejection and acute tubular necrosis. *Nephrol Dial Transplant* 2008; 23: 2666–2672

47. Xiao W, Xu J, Wang Q *et al*. Functional evaluation of transplanted kidneys in normal function and acute rejection using BOLD MR imaging. *Eur J Radiol* 2012; 81: 838–845

48. Liu G, Han F, Xiao W *et al*. Detection of renal allograft rejection using blood oxygen level-dependent and diffusion weighted magnetic resonance imaging: a retrospective study. *BMC Nephrol* 2014; 15: 158

49. Park SY, Kim CK, Park BK *et al*. Evaluation of transplanted kidneys using blood oxygenation level-dependent MRI at 3 T: a preliminary study. *AJR Am J Roentgenol* 2012; 198: 1108–1114

50. Sadowski EA, Fain SB, Alford SK *et al*. Assessment of acute renal transplant rejection with blood oxygen level-dependent MR imaging: initial experience. *Radiology* 2005; 236: 911–919

51. Grabner A, Kentrup D, Schnöckel U *et al*. Non-invasive imaging of acute allograft rejection after rat renal transplantation using 18F-FDG PET. *J Vis Exp* 2013: e4240

52. Djamali A, Sadowski EA, Samaniego-Picota M *et al*. Non-invasive assessment of early kidney allograft dysfunction by blood oxygen level-dependent magnetic resonance imaging. *Transplantation* 2006; 82: 621–628

53. Beckmann N, Cannet C, Fringeli-Tanner M *et al*. Macrophage labeling by SPIO as an early marker of allograft chronic rejection in a rat model of kidney transplantation. *Magn Reson Med* 2003; 49: 459–467

54. Hitchens TK, Ye Q, Eytan DF *et al*. 19F MRI detection of acute allograft rejection with in vivo perfluorocarbon labeling of immune cells. *Magn Reson Med* 2011; 65: 1144–1153

55. Yang D, Ye Q, Williams M *et al*. USPIO-enhanced dynamic MRI: evaluation of normal and transplanted rat kidneys. *Magn Reson Med* 2001; 46: 1152–1163

56. Ye Q, Yang D, Williams M *et al*. In vivo detection of acute rat renal allograft rejection by MRI with USPIO particles. *Kidney Int* 2002; 61: 1124–1135

57. Zhang Y, Dodd SJ, Hendrich KS *et al*. Magnetic resonance imaging detection of rat renal transplant rejection by monitoring macrophage infiltration. *Kidney Int* 2000; 58: 1300–1310

58. Erpicum P, Detry O, Weekers L *et al*. Mesenchymal stromal cell therapy in conditions of renal ischaemia/reperfusion. *Nephrol Dial Transplant* 2014; 29: 1487–1493

59. Aktas A, Karakayali H, Bilgin N *et al*. Serial radionuclide imaging in acute renal allograft dysfunction. *Transplant Proc* 2002; 34: 2102–2105

60. George EA, Codd JE, Newton WT *et al*. Comparative evaluation of renal transplant rejection with radioiodinated fibrinogen 99mTc-sulfur collid, and 67Ga-citrate. *J Nucl Med* 1976; 17: 175–180

61. Lopes de Souza SA, Barbosa da Fonseca LM, Torres Gonçalves R *et al*. Diagnosis of renal allograft rejection and acute tubular necrosis by 99mTc-mononuclear leukocyte imaging. *Transplant Proc* 2004; 36: 2997–3001

62. Grabner A, Kentrup D, Edemir B *et al*. PET with 18F-FDG-labeled T lymphocytes for diagnosis of acute rat renal allograft rejection. *J Nucl Med* 2013; 54: 1147–1153

63. Grabner A, Schnockel U, Kentrup D et al. Strategies for non-invasive molecular imaging of acute allograft rejection by gamma scintigraphy and positron emission tomography. *Curr Radiopharm* 2011; 4: 10–23

64. Aktas A, Aras M, Colak T et al. Indicators of acute rejection on Tc-99m DTPA renal scintigraphy. *Transplant Proc* 2006; 38: 443–448

65. Gupta SK, Lewis G, Rogers KM et al. Quantitative (99m)Tc DTPA renal transplant scintigraphic parameters: assessment of interobserver agreement and correlation with graft pathologies. *Am J Nucl Med Mol Imaging* 2014; 4: 213–224

66. Sanches A, Etchebehere ECSC, Mazzali M et al. The accuracy of (99m)Tc-DTPA scintigraphy in the evaluation of acute renal graft complications. *Int Braz J Urol* 2003; 29: 507–516

67. Niederle P, Reneltová I, Rossmann P et al. Clinical detection of rejection nephropathy using 125I-labelled fibrinogen. *Int Urol Nephrol* 1976; 8: 71–77

68. Salaman JR. Renal transplant rejection detected with 125 I-fibrinogen. *Proc R Soc Med* 1972; 65: 476

69. Smith SB, Wombolt DG. Histologic correlation of transplant rejection diagnosed by computer-assisted sulfur colloid scan. *Urology* 1983; 21: 151–153

70. Petronis JD, Kittur DS, Wilasrusmee C. Critical evaluation of radiolabeled lymphocytes to detect acute renal transplant rejection in a large animal model. *Med Sci Monit* 2002; 8: BR515–BR520

71. Jouret F, Lhommel R, Beguin C et al. Positron-emission computed tomography in cyst infection diagnosis in patients with autosomal dominant polycystic kidney disease. *Clin J Am Soc Nephrol* 2011; 6: 1644–1650

72. Boellaard R, Delgado-Bolton R, Oyen WJG et al. FDG PET/CT: EANM procedure guidelines for tumour imaging: version 2.0. *Eur J Nucl Med Mol Imaging* 2015; 42: 328–354

73. Minamimoto R, Takahashi N, Inoue T. FDG-PET of patients with suspected renal failure: standardized uptake values in normal tissues. *Ann Nucl Med* 2007; 21: 217–222

74. Mettler FA, Huda W, Yoshizumi TT et al. Effective doses in radiology and diagnostic nuclear medicine: a catalog. *Radiology* 2008; 248: 254–263

75. Barrington SF, Mikhaeel NG, Kostakoglu L et al. Role of imaging in the staging and response assessment of lymphoma: consensus of the International Conference on Malignant Lymphomas Imaging Working Group. *J Clin Oncol* 2014; 32: 3048–3058

76. Engel H, Steinert H, Buck A et al. Whole-body PET: physiological and artifactual fluorodeoxyglucose accumulations. *J Nucl Med* 1996; 37: 441–446